#### **PAPER**

# Fabrication and characterization of 3D printing induced orthotropic functional ceramics

To cite this article: Luis A Chavez et al 2019 Smart Mater. Struct. 28 125007

View the article online for updates and enhancements.

## Recent citations

- The Influence of Printing Parameters,
Post-Processing, and Testing Conditions
on the Properties of Binder Jetting Additive
Manufactured Functional Ceramics
Luis A. Chavez et al

Smart Mater. Struct. 28 (2019) 125007 (7pp)

https://doi.org/10.1088/1361-665X/ab4e0a

# Fabrication and characterization of 3D printing induced orthotropic functional ceramics

Luis A Chavez<sup>1,2</sup>, Bethany R Wilburn<sup>1,2</sup>, Paulina Ibave<sup>1,2</sup>, Luis C Delfin<sup>1,2</sup>, Sebastian Vargas<sup>1,2</sup>, Hector Diaz<sup>3</sup>, Christian Fulgentes<sup>4</sup>, Anabel Renteria<sup>1,2</sup>, Jaime Regis<sup>1,2</sup>, Yingtao Liu<sup>5</sup>, Ryan B Wicker<sup>1,2</sup> and Yirong Lin<sup>1,2</sup>

E-mail: lachavez5@miners.utep.edu

Received 16 May 2019, revised 18 August 2019 Accepted for publication 15 October 2019 Published 4 November 2019



#### **Abstract**

The orthotropic functional properties of additively manufactured ceramics due to the fabrication process was characterized in this study. Spherical, environmentally benign barium titanate (BaTiO<sub>3</sub>) powders were fabricated using binder jetting 3D printing. Dielectric and piezoelectric properties of these ceramics were characterized as a function of the printing orientation. The dielectric constant of the samples tested normal to the printing layers was observed to be 20% higher than those tested in the parallel fashion. Similarly, the piezoelectric response was found to be over 35% in the normal orientation. With these results, it was shown that the electroding orientation has a direct influence on the functional properties of additively manufactured ceramics. Overall, with less than 37% of the theoretical density, the average piezoelectric coefficient for the perpendicularly tested ceramics was found to be 152.7 pC N<sup>-1</sup>, which is 80% of the theoretical value. The high piezoelectric response obtained with such low densities can lead to the development of more mass efficient, and cost-effective sensing and energy harvesting devices, as well as structures that can be tuned to respond based on the direction of the loads applied.

Keywords: additive manufacturing, multifunctional ceramics, binder jetting, dielectric, piezoelectric

(Some figures may appear in colour only in the online journal)

### 1. Introduction

Piezoelectric materials have become of great interest across many different industries due to their natural ability to be implemented as sensors [1], energy harvesters [2], and actuators [3]. Piezoelectric materials are of special interest as pressure [4] and temperature [5] sensors under high frequency conditions. Piezoelectric ceramics have gained special interest in the power generation industry as they can withstand the harsh environments present in energy conversion systems [6]

<sup>&</sup>lt;sup>1</sup> Department of Mechanical Engineering, The University of Texas at El Paso, El Paso, TX 79968, United States of America

<sup>&</sup>lt;sup>2</sup> W.M. Keck Center for 3D Innovation, The University of Texas at El Paso, El Paso, TX 79968, United States of America

<sup>&</sup>lt;sup>3</sup> Department of Chemical Engineering, University of Puerto Rico Mayaguez, Mayaguez, PR 00680, United States of America

<sup>&</sup>lt;sup>4</sup> Department of Chemical Engineering, University of California Santa Barbara, Santa Barbara, CA 93106, United States of America

<sup>&</sup>lt;sup>5</sup> Department of Aerospace and Mechanical Engineering, The University of Oklahoma, Norman, OK 73019, United States of America

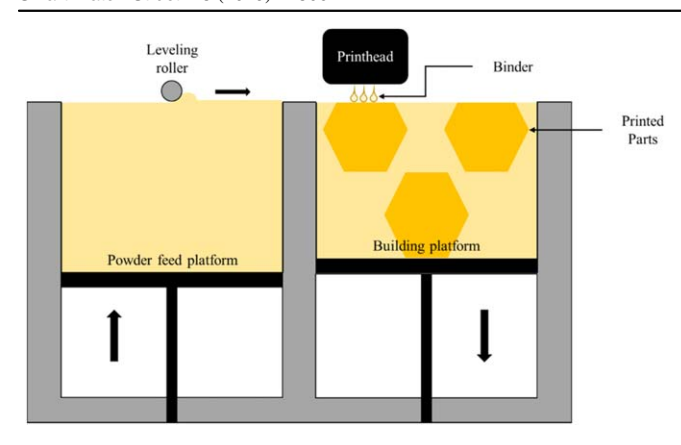


**Figure 1.** Schematic showing the working mechanism of binder jetting additive manufacturing [18].

while providing accurate pressure and temperature sensing. However, despite their innate potential as sensing devices, piezoelectric ceramics also have the same intrinsic drawbacks observed in most ceramics: they are difficult to machine [7], and their brittleness induces low resistivity to fracture [8]. Therefore, producing custom complex geometries with ceramic materials can be almost impossible to achieve through conventional fabrication methods. A proposed method to circumvent this issue is to fabricate complex ceramic parts with additive manufacturing (AM) [9]. A wide array of smart materials and devices has been fabricated in recent years through the use of AM. Among the smart materials fabricated using AM are shape memory polymers [10], polymer-carbon mechanical nanocomposites [11], ceramic-polymer dielectric composites [12], and electrically conductive polymer-carbon nanocomposites [13].

In recent years, efforts to fabricate ceramics using 3D printing (3DP) technology have been made [14]. However, these fabrication efforts often present with a tradeoff between printing resolution [15], material properties [16], and scalability [17]. Among all these promising AM technologies, one of the technologies previously used to produce all-ceramic 3D-printed parts is binder jetting. Binder jetting technology uses a printhead to selectively jet liquid binder onto a powder bed to join powder particles in a layer-by-layer fashion. A schematic depicting binder jetting 3DP technology is provided in figure 1 [18]. Binder jetting can provide high resolution and freedom of design of the printed part, however low densities and pronounced anisotropies of the 3D printed materials are consistently observed when using this technique [19]. The fabrication of piezoelectric devices using 3DP has been successful in the past when the focus of such efforts pertained to their use as fillers for composites [4].

Anisotropic and low-density materials are commonly found in nature and more recently in man-made material systems and structures. One class of materials where a combination of these qualities has been observed are laminate composites. The low densities observed for this type of structures is not seen as a defect in the final part, but instead as an advantage over conventional structural fabrication as their comparable strength to bulk materials yields higher

specific strengths, and more efficient structures as a result [20]. Similarly, anisotropy in composite materials is common since these materials are engineered to specific applications where their properties must be tailored to the loading condition they are subjected to [21]. Composite materials that encompass dielectric and piezoelectric properties for the fabrication of devices have gained significant traction in recent years in fields including the aerospace, automotive, and medical industries [22]. Similar to laminate composites, dielectric and piezoelectric composites take advantage of the properties of their different component materials to create a system with tailored performance. Dielectric composites normally use a polymer matrix with a ceramic filler to take advantage of the manufacturability of the polymer and the high piezoelectric properties from the ceramic filler [23]. Ceramic particles are commonly dispersed throughout the polymer matrix in a random manner, improving the properties of the composite by material selection and manipulation [24].

Despite all the advantages in manufacturability and efficiency that can be obtained from the use of dielectric and piezoelectric composites, they are not ideal for extreme environments where the polymer matrices of the composites cannot survive [25]. Therefore, there is a need to fabricate high-functionality piezoelectric structures that can be tailored for custom applications and do not require the use of polymer matrices. As previously mentioned, AM can provide with the necessary tailoring capabilities. However, structures fabricated using this technique present a great degree of dependence on their properties due to their layer-by-layer fabrication nature. As a result of this, the performance of the polymer [26], metal [27], and cementitious [19] 3D printed parts is highly dependent on their printing direction during the manufacturing process. Consequently, the anisotropic behavior of functional ceramics fabricated by AM should be further studied to enhance the tailoring capabilities of this novel technique.

The anisotropy of 3D printed ceramics was studied in this work using barium titanate (BaTiO<sub>3</sub>). BaTiO<sub>3</sub> is one of the most widely used and studied functional ceramics. BaTiO<sub>3</sub> is a widely used lead-free functional material due to its high dielectric and piezoelectric properties [28]. In this paper, BaTiO<sub>3</sub> was manufactured using binder jetting 3DP to study the feasibility to fabricate functional piezoelectric ceramics. In addition, the impact of the fabrication process in the material properties was characterized and discussed. The orthotropic dielectric and piezoelectric material properties of printed ceramics were measured, and the origin was discussed.

# 2. Methodology

#### 2.1. Sample fabrication

An ExOne M-Lab R1 binder jetting 3D printer as schematically shown in figure 1 was used for the fabrication of the 3D objects. BaTiO<sub>3</sub> spherical powder (The Goodfellow Group, BA506010) with a max. particle size of 45  $\mu$ m was used to

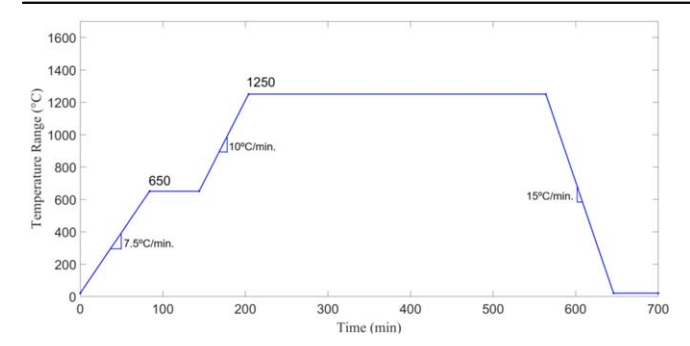


Figure 2. Sintering profile applied to manufactured samples.

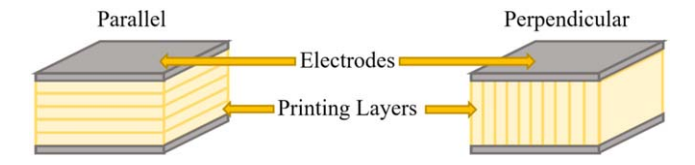


Figure 3. Schematic of sample electroding configurations.

Table 1. Printing parameters used for sample fabrication.

D	<sup>7</sup> alue
Parameter V	arue
Layer thickness ( $\mu$ m) Binder saturation (%) Feed to build ratio Initial spread speed (mm s <sup>-1</sup> )	24.4 135 100 1.75 5

print 12 mm cubes. Additionally, BS004 solvent binder and CL001 cleaner (The ExOne Company, PA, USA) were used for the printing of the functional ceramic components. Printing parameters were selected before initialization of the parts printing as listed in table 1.

#### 2.2. Sample preparation

After printing, the powder bed containing the samples were cured at 200 °C for two hours. The curing process allowed the binder within printed cubes to cure thus retain their shape during the de-powdering process. Once the samples were depowdered, they were submitted to a sintering process as shown in figure 2. First, a binder burnout stage of one hour was introduced at 650 °C to remove any carbon traces from the binding material, this binder burnout stage was followed by a sintering stage of six hours at 1250 °C to densify the printed ceramics [29].

The sintered ceramics were then cut using a diamond cutoff saw. The samples were cut in both the parallel and perpendicular planes to the printing direction in order to study the desired cross-section. The samples were then polished using 400 grit silicon carbide (SiC) pads for initial size reduction and 1200 grit SiC for finer surface finish. The polished surfaces were then electroded using conductive silver paint (SPI supplies, PA, USA). The different sample configurations are shown in figure 3. Heat treatment was applied to the painted samples to evaporate any organic material from the paint. Finally, the samples were poled under a DC electric field of 0.33 kV mm<sup>-1</sup> at a temperature of 60 °C in a silicone oil bath for two hours [30].

#### 2.3. Characterization

The apparent density of the 3D printed parts was characterized by measuring the external volume of the samples and recording the mass of the bodies before and after sintering. Sample morphology and microstructure were investigated using scanning electron microscopy (SEM, Hitachi 4800, Tokyo, Japan). The surfaces of the samples in parallel and perpendicular orientations to the printing layers were characterized and compared.

The electroded samples were used to characterize the dielectric and piezoelectric properties of the 3D printed ceramic. A 1920 Precision LCR meter (IED lab, WI, USA) was used to characterize the capacitance tested at a frequency of 1 KHz to calculate the dielectric constant of the BaTiO<sub>3</sub> samples using equation (1)

$$\varepsilon = \frac{Cd}{A\varepsilon_o},\tag{1}$$

where  $\varepsilon$  denotes the dielectric constant, C denotes capacitance, d denotes the thickness between opposing electrodes, A denotes the area of the electrode, and  $\varepsilon_o$  denotes the permittivity of free space.

Finally, piezoelectric properties of two sets (perpendicular and parallel electroding) of samples was characterized. Piezoelectric characterization was performed by recording the electrical output generated by the sample when a cyclic load was applied using a  $d_{33}$  meter (APC International Ltd, PA, USA).

#### 3. Results and discussion

Barium titanate 3D objects were successfully fabricated using a commercially available binder jetting machine. Densities of six green body samples were obtained using geometrical calculations. The average density of these samples was found to be 1.54 g cm<sup>-3</sup>, or 25.65% of the theoretical density of the material. After the sintering process was performed, the 3D printed parts were found to have an average density of 2.21 g cm<sup>-3</sup>, or 36.77% of the theoretical value. An average shrinkage of 20% was observed in each axis after sintering.

A photograph showing the samples before and after sintering can be seen in figures 4(A), (B) portrays an isometric view of samples to identify the surface finish; (C) shows the sintered sample having a 20% shrinkage value compared to the green body; and (D) shows lattice 3D printed structures produced by the binder jetting technique, which shows the high resolution of manufactured parts with designed geometries.

Based on the low densities observed by the sintered samples, a high level of porosity was expected. The

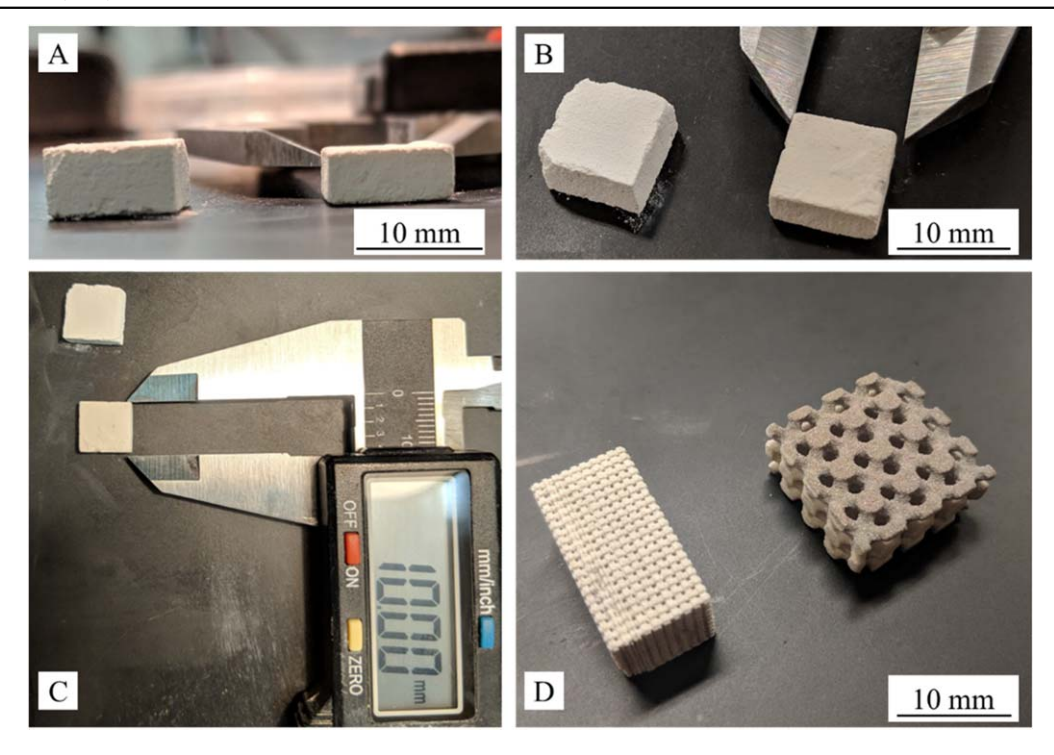
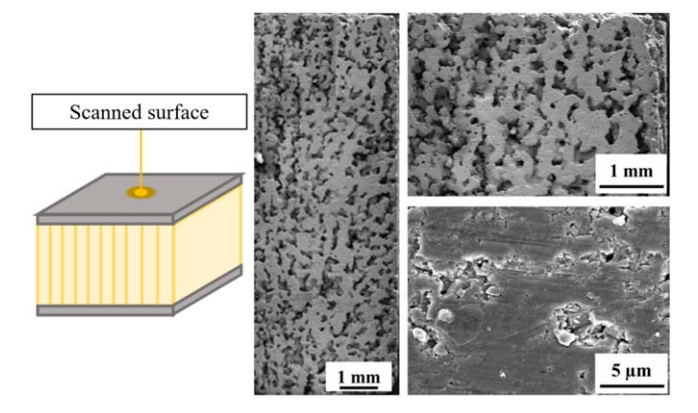


Figure 4. 3D printed samples and geometry complexity achieved using binder jetting technology.



**Figure 5.** SEM micrographs depicting the pore pattern observed on the perpendicular plane.

microstructural morphology of the samples was characterized in the planes parallel and perpendicular to the printing layers. The SEM images showing the cross section of these two types of samples are shown in figures 5 and 6. From these images, it was seen that both sample directions were highly porous. However, distinct characteristics between the two sample orientations were clearly defined.

For the samples characterized perpendicular to the printing layers, figure 5, a uniform height was observed as well as 'patterned' pores, which is consistent with the printing layers. In contrast, the samples parallel to the layer-by-layer deposition lack the distinction of pore alignment and have a flat surface. These characteristics are consistent with the morphology expected when looking at a printing layer. The packing of the layers in the different orientations also had distinctive characteristics. There was relatively high particle packing in the 'printing layers,' while low powder packing

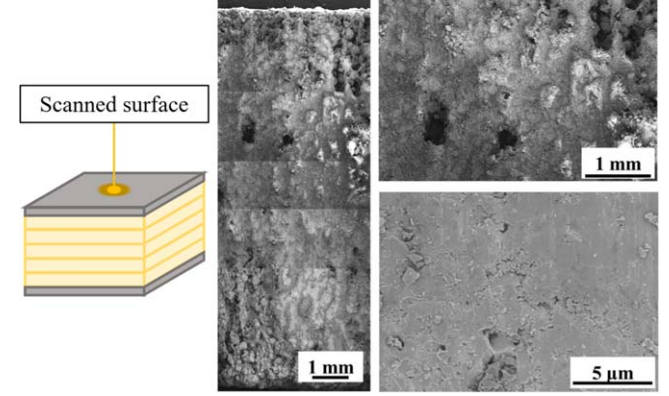


**Figure 6.** SEM micrographs of a uniform 3D printed layer, commonly observed in the parallel plane.

between the layers. This difference in particle packing was an artifact from the fabrication process, and not the powder interaction.

As a result of the high porosity, and characteristic pore arrangement, a high level of anisotropy was observed in the functional properties of the 3D printed objects. After testing the dielectric properties in the orientations parallel and perpendicular to the printing layers, a significant difference was observed in the dielectric constant of the different sample groups, as shown in figure 7.

For the samples that were electroded in a parallel manner to the printing layer, an average dielectric constant of 581.6 was observed. In contrast, the group of samples electroded in the perpendicular plane to the printing orientation presented an average dielectric constant of 698. This represents a 20% improvement in the average performance of the perpendicular

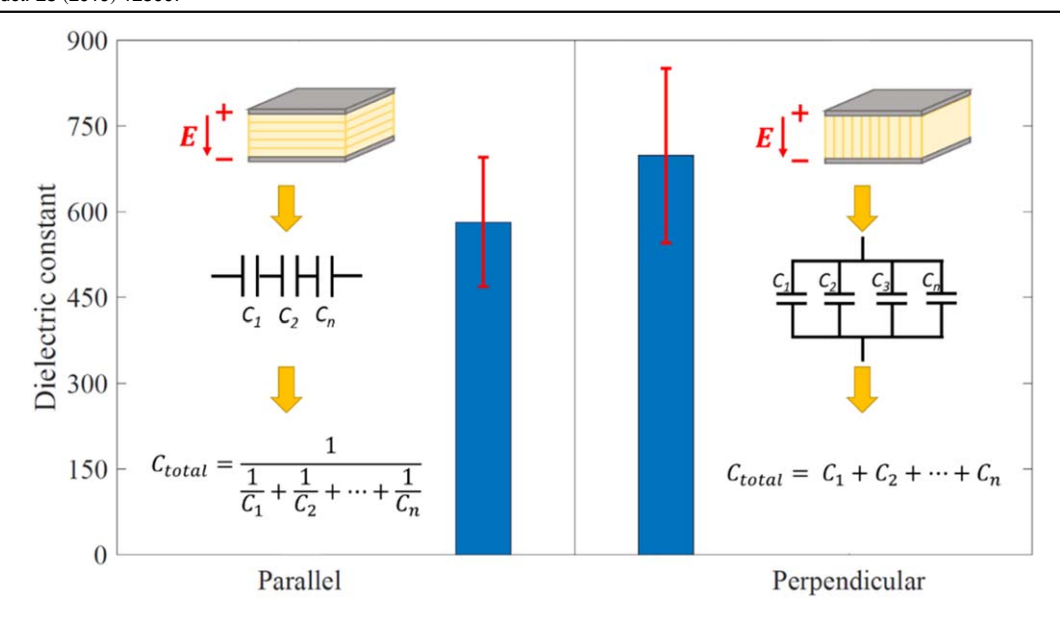


Figure 7. Comparison of average dielectric constant and standard deviation at 1 kHz.

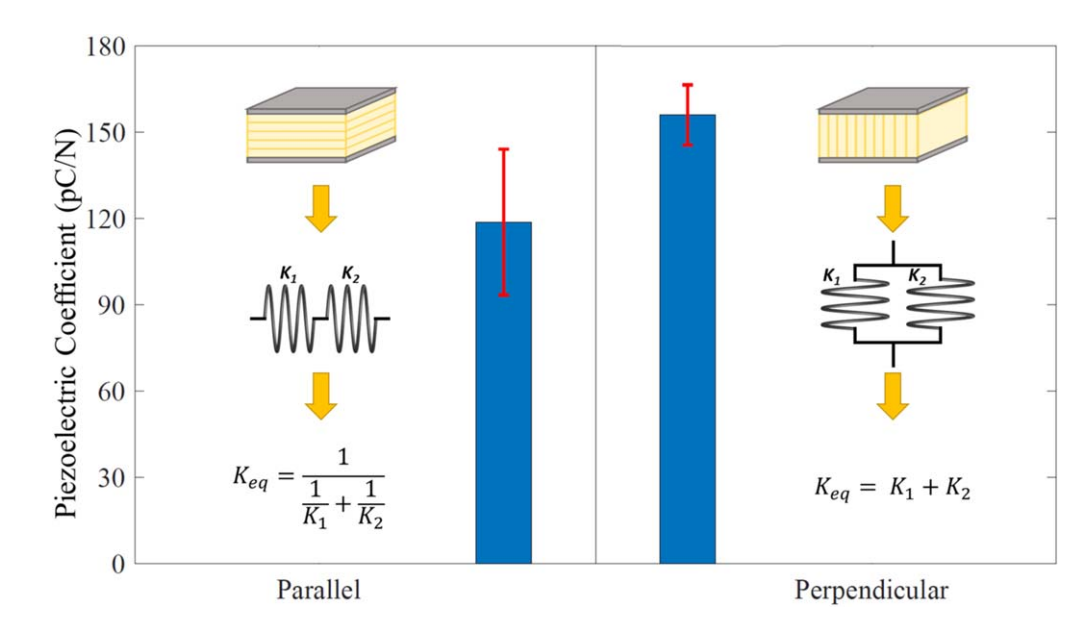


Figure 8. Comparison of piezoelectric coefficients and standard deviation between sample orientations.

set of samples over the ones electroded in the parallel direction.

This dielectric property dependence on the printing direction can be attributed to the morphology of the sample and printing layers, and the equivalent capacitor circuit that these formed in the different samples as shown in figure 7. In the case of the samples tested in the parallel direction, air pockets are formed in between the layers of the high dielectric material, creating a set of capacitors arranged in a series circuit. Due to the low dielectric constant of air, this type of arrangement will inhibit the dielectric capacitance of the system, lowering the overall dielectric property in the system. In contrast, the perpendicularly tested samples created a set of capacitors arranged in a parallel circuit, and therefore the presence of air in between the layers did not have a negative impact on the dielectric performance of this sample set.

Similarly, a dependence on the fabrication orientation was observed for the piezoelectric properties. The average piezoelectric charge coefficient for the parallel samples was found to be  $113~{\rm pC}~{\rm N}^{-1}$ . Meanwhile, the piezoelectric charge coefficient for the perpendicular set was  $152.7~{\rm pC}~{\rm N}^{-1}$ . This difference in piezoelectric performance represented an improvement of 35.1% over the parallely tested group. A comparison of the piezoelectric properties for these sample sets as well as the observed standard deviation are shown in figure 8.

This influence of the printing direction on the piezoelectric properties can be attributed to the load transfer difference between these two electroding arrangements. For parallel electroding, mechanical loading was absorbed by the defects between printing layers thus leaving the active piezoelectric ceramic not excited. While for perpendicular electroding, mechanical loads were carried and transferred better through the ceramic more due to higher mechanical stiffness of the ceramics [19] and less voids to interrupt this loads.

Because of these higher mechanical properties of printed ceramics, a higher amount of mechanical loading was transferred to the piezoelectric ceramic layers, allowing more mechanical stresses to be converted to electrical signals. Therefore, the piezoelectric charge coefficient was found to be higher using perpendicular electroding format. Overall, an average piezoelectric charge coefficient of 80% of the theoretical value reported for BaTiO<sub>3</sub> ceramics with samples only 36.77% dense was obtained [31].

#### 4. Conclusion

Binder jetting 3DP was utilized to fabricate BaTiO<sub>3</sub> samples with high piezoelectric charge coefficients. The 3D printed ceramic presented a piezoelectric coefficient of 80% of the theoretical value with density a relative density of only 36.77%. A direct correlation between the fabrication orientation, and the functional properties of the ceramic was observed. The dielectric and piezoelectric capabilities were shown to be dependent on the orientation of the layer-by-layer fabrication process, where there was an increase in the performance of the samples tested in the orientation normal to the printing layers.

The average dielectric properties of the perpendicularly tested samples were found to be 20% higher than those parallel to the printing orientation, achieving an average dielectric constant of 698 and 581.6 respectively. Additionally, piezoelectric properties were found to have a strong dependence on the printing direction. Samples tested in the parallel direction presented a piezoelectric charge coefficient of 113 pC N<sup>-1</sup>, while the perpendicular samples presented an improvement of 35.1%. The piezoelectric charge coefficient obtained for the perpendicular samples was 152.7 pC N<sup>-1</sup>, which represents 80% of the theoretical piezoelectric properties of ceramic BaTiO<sub>3</sub>.

#### **Acknowledgments**

This research is funded by Department of Energy (DOE) under Grant No. DE-FE0027502, and DE-NA0003865, as well as by the DOE National Nuclear Security Administration (NNSA) under Grant No. DE-NE-0003865. Their financial support is greatly appreciated.

# **ORCID** iDs

Luis A Chavez https://orcid.org/0000-0001-5203-6708 Anabel Renteria https://orcid.org/0000-0001-9013-8115 Yingtao Liu https://orcid.org/0000-0002-6232-9704

#### References

- [1] Sodano H A, Inman D J and Park G 2004 A review of power harvesting from vibration using piezoelectric materials Shock Vib. Dig. 36 197–206
- [2] Chavez L A, Jimenez F O Z, Wilburn B R, Delfin L C, Kim H, Love N and Lin Y 2018 Characterization of thermal energy harvesting using pyroelectric ceramics at elevated temperatures *Energy Harvesting Syst.* 5 3–10
- [3] Ma M, Wei X, Shu X and Zhang H 2019 Producing solder droplets using piezoelectric membrane-piston-based jetting technology J. Mater. Process. Technol. 263 233–40
- technology *J. Mater. Process. Technol.* **263** 233–40

  [4] Kim H, Torres F, Villagran D, Stewart C, Lin Y and Tseng T L B 2017 3D printing of BaTiO3/PVDF composites with electric *in situ* poling for pressure sensor applications *Macromol. Mater. Eng.* **302** 1700229
- [5] Zhang S and Yu F 2011 Piezoelectric materials for high temperature sensors J. Am. Ceram. Soc. 94 3153–70
- [6] Chavez L A, Elicerio V F, Regis J E, Kim H, Rosales C A G, Love N and Lin Y 2018 Thermal and mechanical energy harvesting using piezoelectric ceramics *Mater. Res. Express* 6 025701
- [7] Yonghong L, Zhixin J and Jinchun L 1997 Study on hole machining of non-conducting ceramics by gas-filled electrodischarge and electrochemical compound machining J. Mater. Process. Technol. 69 198–202
- [8] Cook R F, Freiman S W, Lawn B R and Pohanka R C 1983 Fracture of ferroelectric ceramics Ferroelectrics 50 267–72
- [9] Gao W, Zhang Y, Ramanujan D, Ramani K, Chen Y, Williams C B and Zavattieri P D 2015 The status, challenges, and future of additive manufacturing in engineering *Comput.-Aided Des.* 69 65–89
- [10] Garcia Rosales C A, Kim H, Garcia Duarte M F, Chavez L, Castañeda M, Tseng T L B and Lin Y 2018 Characterization of shape memory polymer parts fabricated using material extrusion 3D printing technique *Rapid Prototyping J.* 25 322–31
- [11] Chavez L A, Regis J E, Delfin L C, Rosales C A, Kim H, Love N and Lin Y 2019 Electrical and mechanical tuning of 3D printed photopolymer–MWCNT nanocomposites through in situ dispersion J. Appl. Polym. Sci. 136 47600
- [12] Castles F, Isakov D, Lui A, Lei Q, Dancer C E J, Wang Y and Grant P S 2016 Microwave dielectric characterisation of 3Dprinted BaTiO<sub>3</sub>/ABS polymer composites Sci. Rep. 6 22714
- [13] Postiglione G, Natale G, Griffini G, Levi M and Turri S 2015 Conductive 3D microstructures by direct 3D printing of polymer/carbon nanotube nanocomposites via liquid deposition modeling *Composites* A 76 110–4
- [14] Travitzky N, Bonet A, Dermeik B, Fey T, Filbert-Demut I, Schlier L and Greil P 2014 Additive manufacturing of ceramic-based materials Adv. Eng. Mater. 16 729–54
- [15] Kim H, Renteria-Marquez A, Islam M D, Chavez L A, Rosales C A, Ahsan M A and Lin Y 2018 Fabrication of bulk piezoelectric and dielectric BaTiO<sub>3</sub> ceramics using paste extrusion 3D printing technique *J. Am. Ceram. Soc.* 102 3685–94
- [16] Du W, Ren X, Ma C and Pei Z 2017 Binder jetting additive manufacturing of ceramics: a literature review Volume 14: Emerging Technologies; Materials: Genetics to Structures; Safety Engineering and Risk Analysis (https://doi.org/ 10.1115/imece2017-70344)
- [17] Derby B 2011 Inkjet printing ceramics: From drops to solid J. Eur. Ceram. Soc. 31 2543–50
- [18] Gaytan S M, Cadena M A, Karim H, Delfin D, Lin Y, Espalin D and Wicker R B 2015 Fabrication of barium titanate by binder jetting additive manufacturing technology *Ceram. Int.* 41 6610–9

- [19] Feng P, Meng X, Chen J F and Ye L 2015 Mechanical properties of structures 3D printed with cementitious powders Constr. Build. Mater. 93 486–97
- [20] Dong S, Li J F and Viehland D 2004 Characterization of magnetoelectric laminate composites operated in longitudinal-transverse and transverse–transverse modes J. Appl. Phys. 95 2625–30
- [21] Castellanos A G, Islam M S, Shuvo M A I, Lin Y and Prabhakar P 2018 Nanowire reinforcement of woven composites for enhancing interlaminar fracture toughness J. Sandwich Struct. Mater. 20 70–85
- [22] Kapuria S, Kumari P and Nath J K 2010 Efficient modeling of smart piezoelectric composite laminates: a review Acta Mech. 214 31–48
- [23] Kim H, Wilburn B R, Castro E, Garcia Rosales C A, Chavez L A, Tseng T L B and Lin Y 2018 Multifunctional SENSING using 3D printed CNTs/BaTiO<sub>3</sub>/PVDF nanocomposites J. Compos. Mater. 53 1319–28
- [24] Cui C, Baughman R H, Iqbal Z, Kazmar T R and Dahlstrom D K 1999 *US Patent No.* 5,951,908
- [25] Hanu L G, Simon G P, Mansouri J, Burford R P and Cheng Y B 2004 Development of polymer-ceramic

- composites for improved fire resistance *J. Mater. Process. Technol.* **153** 401–7
- [26] Lee C S, Kim S G, Kim H J and Ahn S H 2007 Measurement of anisotropic compressive strength of rapid prototyping parts J. Mater. Process. Technol. 187 627–30
- [27] Deng D, Moverare J, Peng R L and Söderberg H 2017 Microstructure and anisotropic mechanical properties of EBM manufactured Inconel 718 and effects of post heat treatments *Mater. Sci. Eng.* A 693 151–63
- [28] Acosta M, Novak N, Rojas V, Patel S, Vaish R, Koruza J and Rödel J 2017 BaTiO<sub>3</sub>-based piezoelectrics: fundamentals, current status, and perspectives Appl. Phys. Rev. 4 041305
- [29] Karaki T, Yan K and Adachi M 2007 Barium titanate piezoelectric ceramics manufactured by two-step sintering *Japan. J. Appl. Phys.* 46 7035
- [30] Roberts S 1947 Dielectric and piezoelectric properties of barium titanate *Phys. Rev.* **71** 890
- [31] Berlincourt D and Jaffe H 1958 Elastic and piezoelectric coefficients of single-crystal barium titanate *Phys. Rev.* 111 143